Study of electron impact excitation of argon in the extreme ultraviolet: emission cross section of resonance lines of Ar I, Ar II

1990 J. Phys. B: At. Mol. Opt. Phys. 23 4355

(http://iopscience.iop.org/0953-4075/23/23/017)

J. Phys. B: At. Mol. Opt. Phys. **23** (1990) 4355–4376. Printed in the UK

Study of electron impact excitation of argon in the extreme ultraviolet: emission cross section of resonance lines of Ar I, Ar II

Joseph M Ajello†, Geoffrey K James†, Brian Franklin† and Simon Howell‡

† Jet Propulsion Laboratory, California Institute of Technology, Pasadena, CA 91109, USA

‡ Physics Department, University of Manchester, Manchester M13 9PL, UK

Received 22 June 1990

Abstract. We have studied in a crossed-beam experiment under optically thin conditions the extreme ultraviolet (EUV) spectrum of argon produced by electron impact excitation. The most prominent features of the EUV spectrum between 40 and 110 nm are the resonance lines of Ar I at 104.8 nm and 106.7 nm and of Ar II at 91.96 nm and 93.21 nm. Absolute cross sections of these lines at 200 eV are measured by the relative-flow technique and compared with previous estimates. The measured emission cross section values at 200 eV for the Ar I lines at 104.8 nm and 106.7 nm are 23.1×10^{-18} cm^2 and 9.32×10^{-18} cm^2, respectively, with an uncertainty of 14%. When compared with electron energy loss estimates of the direct excitation cross section these values establish that cascading is larger for the Ar I resonance lines than previous emission experiments have indicated. In addition all the emission cross sections for the Ar I, II Rydberg series in the EUV spectral interval are measured at 0.5 nm resolution. The far ultraviolet (FUV) spectrum of Ar is also surveyed for the first time and is found to consist of Ar II multiplets from simultaneous ionization–excitation.

1. Introduction

We have completed a study of the combined EUV from 40 to 110 nm and FUV from 120 to 210 nm spectral regions by electron impact induced fluorescence of Ar. We have measured the cross sections of the resonance lines of Ar I and II. The 104.8 nm and 106.7 nm resonance lines of Ar I and 91.98 nm and 93.21 nm resonance lines of Ar II represent the transitions between the lowest lying electronic excited states and the ground state of the atom and ion, respectively. These lines will be strongly excited in astrophysical and laboratory weakly ionized plasma regimes containing Ar. The detection of the Ar I resonance lines in circumstellar objects has been designated as a prime objective of EUV space telescopes to help identify planetary formation. Both electron impact excitation and photoexcitation processes are found in space applications. For example electron impact excitation is a strong source of EUV emission in the extended atmospheres of the outer planets (Broadfoot *et al* 1979, 1986, Sandel *et al* 1982) and a careful search for Ar in the atmospheres of the outer planets and their satellites will be made, based on the results presented here using UV planetary

0953-4075/90/234355+22$03.50

observational data already in hand. From a theoretical point of view the *ab initio* calculation of excitation cross sections is served by having laboratory cross sections available for comparison (Sawada *et al* 1971, da Paixao *et al* 1984). Recent measurements of the emission cross section of the Ar II 91.98 nm ionization–excitation transition by two different laboratories (Forand *et al* 1988, McPherson 1984) differ by nearly 50%. Since this transition has been established as a candidate for a benchmark photoemission cross section calibration standard (Risley and Westerveld 1989, van der Burgt *et al* 1989) a new measurement of this cross section is warranted. In addition since this cross section is the basis for the most recent measurement of the emission cross section of the Ar I resonance lines (Forand *et al* 1988) the value of the cross section of the resonance lines may be subject to considerable change.

The most recent survey of emission cross section measurements for the four resonance transitions Ar I 104.8 nm, 106.7 nm, Ar II 91.98 nm, 93.21 nm evaluated in this experiment has been published by van de Bergt *et al* (1989). The Ar II lines arise from inner-shell ionization–excitation. At the same time Li *et al* (1988b) have reviewed the electron energy loss measurements of the Ar I resonance lines (4s, 4s′ states) while presenting their own direct excitation cross section energy loss results. In a subsequent paper Li *et al* (1988a) report emission cross sections of the Ar II resonance lines. Unfortunately, they base the emission cross section of the Ar II resonace lines on the electron energy loss cross sections of the Ar I resonance line, assuming that the cascade cross section is zero at 500 eV, i.e. the emission cross section is equal to the direct excitation cross section for Ar I 106.7 nm. The authors realized that this assumption may be incorrect and recommend accurate emission measurements to renormalize the Ar II 91.98 and 93.21 nm cross sections. The most important results of Li *et al* (1988b) are the measurement of the oscillator strengths of the $3p^6\ {}^1S_0$–$3p^5$ $({}^2P^o_{1/2})4s'$, $({}^2P^o_{3/2})4s$ transitions by extrapolation of the differential cross sections to zero momentum transfer and the measurement of direct excitation cross sections to these states at 400 and 500 eV. This energy range complements the low-energy studies of Chutjian and Cartwright (1981) made between 16 and 100 eV.

The problem of specifying the contribution made by the cascade cross section to the upper states for the 104.8 and 106.7 nm lines is amplified in the recent paper by Forand *et al* (1988, hereafter referred to as F88). In that paper F88 compare their results to McPherson (1984, hereafter referred to as M84). The F88 results for the resonance lines reflect a ratio of 2.41 for the value of the 104.8 nm/106.7 nm cross section ratios at 200 eV. Assuming the Born appproximation is valid in this region, this ratio is nearly the ratio of the oscillator strengths if there is truly negligible cascade. However, Li *et al* (1988b) measure the ratio of oscillator strengths to be 3.83. This fundamental difference in cross section ratios between electron energy loss results and emission results has been repeated several times over the past 15 years. Compare, for example, the electron energy loss results of Li *et al* (1988b) and Chutjian and Cartwright (1981) with the emission cross section results of McConkey and Donaldson (1973), Mentall and Morgan (1976) and F88. F88 were able to show that these two ratios were self-consistent with their emission cross section results at 200 eV if they assumed zero cascade contribution for the 104.8 nm cross section and a 40% cascade contribution to the 106.7 nm cross section. However, there is no evidence to support this assumption, and the emission cross section results of F88 are likely to be too small. The combination of physical processes allowing negligible cascading to the 4s′ state would be extremely fortuitous considering the many dipole-allowed transitions (both one step and two step) to the 4s′ state from ns', np' and nd' Rydberg series. These

transitions along with their lifetimes are indicated in Wiese *et al* (1969). Significant excitation of these higher levels has been found from transitions observed in previously published EUV emission spectra (Lawrence, 1969, McConkey and Donaldson 1973).

Previous work on Ar in the EUV consisted of lifetime measurements of the resonance lines and multiplets of Ar II, III, IV in a pulsed electron beam experiment (Lawrence 1969). The Ar II resonance lines originating from the lowest-lying electronically excited states were found to be free of cascading to 1% or better because of autoionization effects in the cascading levels. McConkey and co-workers in a series of papers dating back to 1973 (McConkey and Donaldson 1973, Tan *et al* 1974, Tan and McConkey 1974a, b, Dassen *et al* 1977, Khakoo and McConkey 1986, F88) have studied Ar by electron impact. McConkey and Donaldson (1973) carefully measured polarization free excitation functions from 0–2 keV; and Dassen *et al* (1977) measured polarization factors from 0 to 500 eV for the Ar I resonance lines. Tan and McConkey (1974a, b) and Tan *et al* (1974) carried out studies of polarization-free excitation functions of the simultaneous ionization and excitation of the $3s3p^6\ ^2S$, $3s^23p^44s\ ^2P$, ns, $nd\ ^2S$, $^{2,4}P$, $^{2,4}D$, $^{2,4}F$ levels of Ar II. Simultaneous ionization and excitation is optically forbidden whenever it involves a two-electron process. An optically forbidden process yields a Bethe–Born plot of zero slope. However the ionization–excitation of the $3s3p^6$ configuration for the 91.98 and 93.21 nm multiplets is a one-electron process with a single 3s electron ejected from the inner shell and by itself this process should yield a positive slope. Three Ar II configurations ($3s3p^6$, $3s^23p^4\ 3d'$ and $3s^2\ 3p^44d'$) are shown to be strongly coupled by configuration interaction with the latter two configurations requiring excitation by a two-electron process. The results of this coupling on the shape of the 91.98 nm and 93.21 nm excitation functions have been discussed by Tan *et al* (1974).

Our goals in this study are fourfold: (i) to settle the controversy over the values of the cross sections for the 91.98 nm, 93.21 nm resonance lines at 200 eV from simultaneous ionization and excitation of Ar; (ii) to measure optically thin spectra of Ar in the EUV in order to obtain cross sections at 200 eV of the Ar I Rydberg series and provide accurate cascading estimates to the $4s'[1/2]_1^0\ ^1P_1$ and $4s\ [3/2]_1^0\ ^3P_1$ levels, the upper states of the 104.8 nm and 106.7 nm resonance transitions, respectively; (iii) to measure excitation functions of the 91.98 nm and 93.21 nm Ar II transitions from 0 to 2 keV and use the McConkey and Donaldson polarization-free excitation function relative shapes from 0 to 2 keV of the 104.8 nm and 106.7 nm Ar I transitions; and (iv) to obtain a spectrum in the FUV of Ar from 120–200 nm with identifications and upper limits to the Ar II multiplets (Kelly 1987).

2. Experimental

The experimental apparatus and VUV calibration techniques have been described in detail in earlier publications (Ajello *et al* 1982, 1984, 1988, 1989, Ajello and Shemansky 1985, Shemansky *et al* 1985a, b). In brief there are two independent experimental systems used in the present measurements with differing spectral resolutions. Each of these systems consists of an electron impact collision chamber in tandem with either an EUV spectrometer which operates from 40 to 140 nm or a FUV spectrometer which operates from 110 to 300 nm. One system is a high-resolution apparatus which was recently described for the first time in a paper (Ajello *et al* 1989) relating cross sections of N_2 in the EUV and has a resolution capability on repeated scans of 0.03 nm. The

other system is a low-resolution apparatus with a spectral resolution of 0.4 nm which has been employed in this laboratory in the earlier papers cited above. Both systems were employed to take cross section data and spectra.

A magnetically collimated beam of electrons is crossed with a beam of gas formed by a capillary array at a background pressure that can be varied from 1×10^{-8} to 3×10^{-4} Torr. The energy resolution is 0.3 eV. The instrument is entirely automated for repetitive scans and interfaced with a computer. There have been three major improvements to the existing electron spectrometer for both the low-resolution and high-resolution systems. First, the collision chamber of both systems and the two UV spectrometers of the low-resolution apparatus have been equipped with turbo pumping systems. The turbo systems have decreased the ultimate vacuum pressure to the 10^{-9} Torr scale.

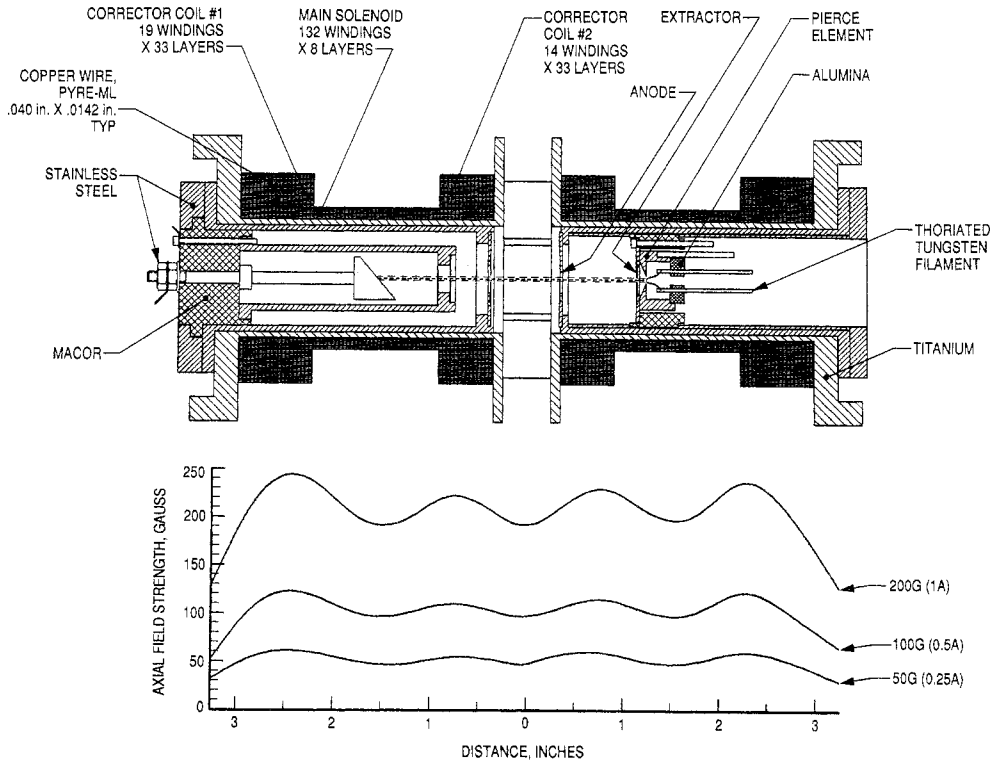

Figure 1. Assembly drawing of the electron gun used in this study. The beam is collimated by a computer-optimized solenoid. The solenoid with corrector coils and measured magnetic field are shown to scale.

Secondly, the quadrupole magnetic configuration described in Ajello *et al* (1988) has been replaced with a solenoid system. The solenoid is shown in figure 1 along with the measured magnetic field. A computer program optimizes the axial magnetic field for uniformity over the finite length (17 cm) by providing corrector coils at the centre and ends. The centre corrector coil corrects for the centre annulus of the solenoid removed for viewing the collision region. The end corrector coils provide for the finite length. For a current of 0.5 A the program predicts a 15% variation of axial magnetic field with minima at the centre and ends and a predicted field strength of 0.01 T.

The measured axial magnetic field had a uniformity of 21% with a mean value of the predicted 0.01 T. The wire used was number 22 wire in rectangular form for ease of winding. The high-vacuum-compatible wire for the measured operating temperature of 117°F is coated with a polyimide with a Dupont trade name of PYRE-ML.

Thirdly the electronics for the electron gun were redesigned to allow for high-voltage programming of the electron accelerating energy from 0 to 2 keV in order to extend our range of operation into the Born region for the first time. An integrated high-voltage system has been developed that provides the necessary high slewing rates together with precision lens and filament voltages over the entire energy range with constant Faraday cup current. There are no commercially available systems capable of providing the range and number of voltages required for this application. The Faraday cup has been redesigned to allow for 100% efficient collection of the electron beam at the 2 keV accelerating energy. The electron gun is shown schematically in figure 1. A schematic of the high-voltage system is shown in figure 2.

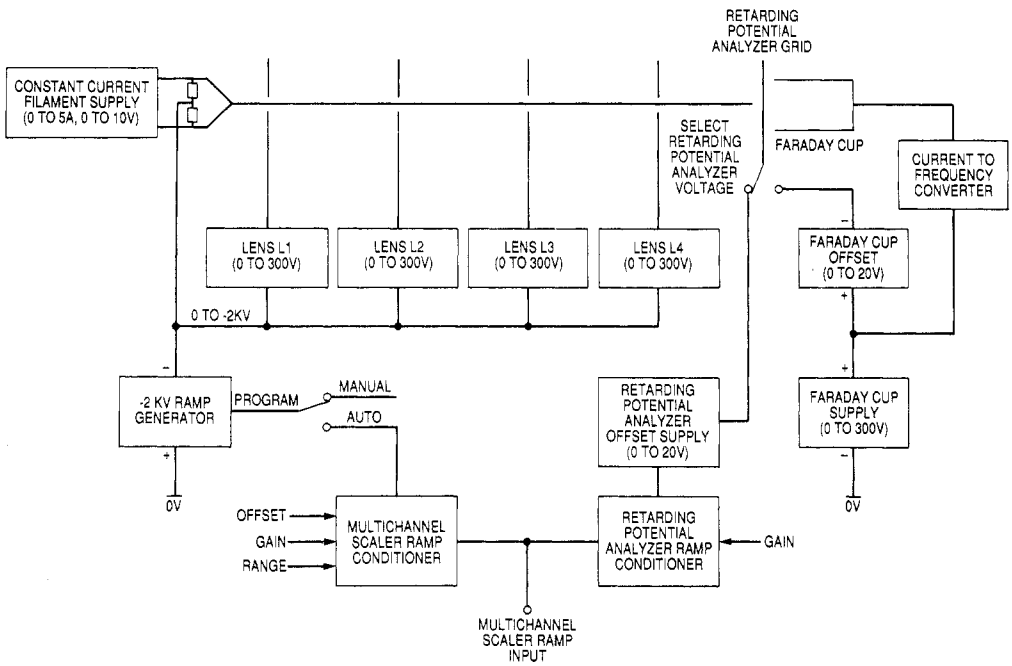

Figure 2. Block diagram of the electronics for the high-voltage (0–2 keV) ramp and electron gun lens power supplies. The retarding potential analyser (RPA) grid and electronics are also shown.

The calibration technique in the EUV is described by Ajello *et al* (1988). This calibration technique in the wavelength range between 80 and 120 nm, based on the molecular H_2 excitation, produces a root sum square uncertainty in the emission cross section of 14% from 90–120 nm and 22% from 80–90 nm . The uncertainty is a combination of three principal uncertainties: (i) relative calibration uncertainty of 10% (90–120 nm) or 20% (80–90 nm) (Ajello *et al* 1988); (ii) absolute calibration uncertainty of 10% for the N I (120 nm) emission cross section (Ajello *et al* 1989, Ajello and Shemansky 1985); and (iii) signal statistics of 3%. The calibration technique below

80 nm generates larger experimental errors for emission cross sections. The root sum square uncertainty of the cross sections below 80 nm is 35%.

The measurements reported here were made at an angle of 90° between electron beam axis and optic axis. The Ar II resonance lines (^2S–$^2P_{1/2,3/2}$) are unpolarized and unaffected by self-absorption. However the Ar I resonance lines are strongly polarized as measured by Dassen *et al* (1977). The polarization is zero at 200 eV. For this reason we study the electron impact induced fluorescence spectrum of Ar at 200 eV. We measure the polarization-free excitation function of the Ar II lines from 0 to 2 keV and we renormalize the polarization-free excitation function of the Ar I lines of McConkey and Donaldson (1973).

3. The EUV spectrum

The calibrated optically thin EUV electron impact induced fluorescence spectrum of Ar at 200 eV is shown in figure 3 at a resolution of 0.5 nm. The gas foreground abundance of Ar in the collision chamber at a background pressure of 3×10^{-8} Torr is 1.6×10^{10} cm^{-2}. The optical thickness of the medium for Ar(104.8 nm), the strongest Ar I resonance line, at line centre is 0.016 at a gas temperature of 300 K. Self-absorption corrections to other resonance lines in the ns, ns' Rydberg series are negligible. A total of 29 first-order features are shown in figure 3. A digital listing of the identifications and cross sections is given in table 1. The absolute cross sections are based on the relative-flow results for the Ar II(919.8 nm) line. Comparisons with other works are given in the last column of table 1. All the features are identified as Ar I, II and III The identifications are taken from Kelly (1987). Below 80 nm the agreement of our cross section values for the Ar II multiplets at feature numbers 3, 5, 6, 8 and 12 with the results of Tan *et al* (1974) is quite good and within the combined experimental error bars. The disagreement with the corrected cross sections of Mentall and Morgan (1976) is quite substantial over the entire wavelength range 40 and 110 nm for feature numbers 16, 24, 25, 26, 27, 28 and 29. The cross sections of Ar I, II, III transitions associated with other feature numbers have not been reported previously.

The results for features with wavelengths above 80 nm in table 1 are particularly important because the comparison with most other measurements occurs in this wavelength range. The present results and the M84 result are in excellent agreement for the Ar II (91.98 nm) transition and differ from the F88 result by nearly 50%. This result has important ramifications for the Ar I resonance lines. Our results for the 104.8 nm and 106.7 nm lines are substantially larger than any previous emission cross section measurement, indicating substantial cascading to both lines. Thus the only previous results in table 1 that used a reliable method for estimating Ar I emission cross sections are those that do not assume zero cascading. Only F88 and Mentall and Morgan (1976) do not base their absolute cross sections on the Born approximation. Our cross section ratio for 104.8 nm/106.7 nm is 2.48, in close agreement with F88 (2.41) and Mentall and Morgan (2.44). Thus the difference between the three results is one of absolute calibration. Emission cross section results from other publications have erroneously assumed small cascading to either one of the resonance lines or both. For example McConkey and Donaldson use the Born approximation. F88 use the same calibration technique presented here but find emission cross sections that require negligible cascading to the 104.8 nm line. At the same time the discussion of Li *et al* (1988a, b) attempts to compare direct excitation cross sections and emission

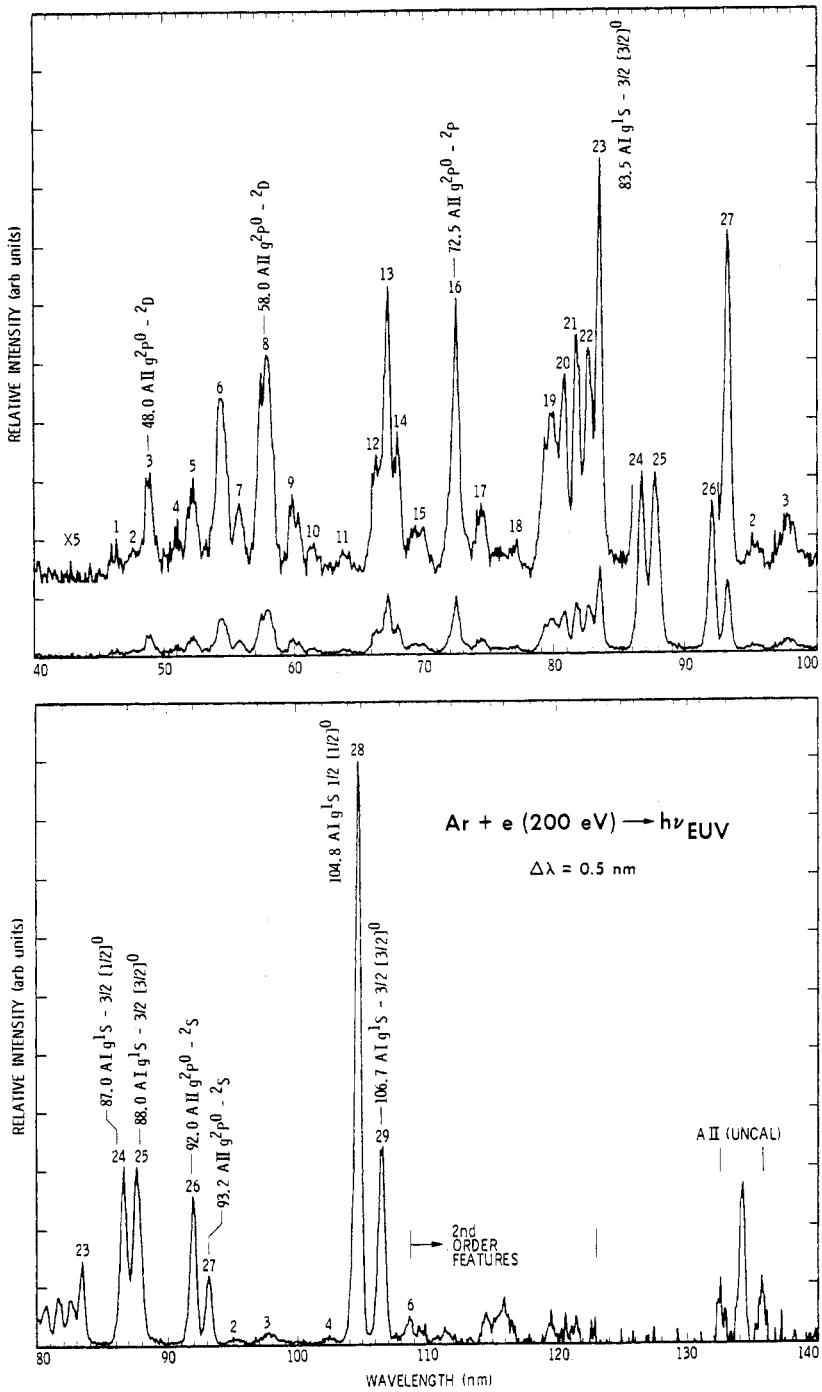

Figure 3. Calibrated, optically thin electron impact induced fluorescence spectrum at 200 eV impact energy at a resolution of 0.5 nm. The spectrum was obtained in the crossed-beam mode at 3×10^{-8} Torr background pressure. All of the numbered features are identified in table 1.

Table 1. Ar emission cross sections at 200 eV. λ_{obs} is the observed peak wavelength and IWI the integrated wavelength interval. Cross sections and the other measurements (final column) are given in 10^{-18} cm^2. *, allowed transitions of Ar I and Ar II; st, standard line (proposed by Kelly 1987); +, strongest component of feature; Δ, corrected for self-absorption effect of 1.6% using oscillator strengths of Li *et al* (1988b).

No	Species	Wavelength (nm)	Term*	λ_{obs} (nm)	IWI (nm)	Cross section 200 eV	Other expts
1	Ar I	45.044	Unclassified	46.6	44.8–46.8	0.29	
	Ar II	46.583 65 st	$g^2P^o-{}^2D$				
2	Ar II	46.963 01 st	$g^2P^o-{}^2D$	47.6	46.8–47.8	0.34	
	Ar II	47.281 14 st	$g^2P^o-{}^2D$				
	Ar II	47.590 54 st	$g^2P^o-{}^2D$				
	Ar II	47.710 48 st	$g^2P^o-{}^2P$				
	Ar II	47.760 68 st	$g^2P^o-{}^2F$				
	Ar II	47.916 78 st	$g^2P^o-{}^4P$				
	Ar II	47.921 77 st	$g^2P^o-{}^4F$				
	Ar II	47.081 08 st	$g^2P^o-{}^2D$				
3	Ar II	48.244 51 st	$g^2P^o-{}^4P$	48.9	47.8–49.8	1.15	1.28[b]
	Ar II	48.722 72 st	$g^2P^o-{}^2S$				
	Ar II	48.879 26 st	$g^2P^o-{}^2D$				
	Ar II	48.896 15 st	$g^2P^o-{}^2P$				
	Ar II	48.919 53 st	$g^2P^o-{}^2D$				
	Ar II	49.064 95 st	$g^2P^o-{}^2S$				
	Ar II	49.070 12 st	$g^2P^o-{}^2P$				
	Ar II	49.240 83 st	$g^2P^o-{}^2P$				
	Ar II	49.264 54 st	$g^2P^o-{}^2D$				
	Ar II	49.466 76 st	$g^2P^o-{}^2F$				
4	Ar II	49.665 92 st	$g^2P^o-{}^4P$	51.0	49.8–51.4	0.44	
	Ar II	49.991 92 st	$g^2P^o-{}^2P$				
	Ar II	50.080 16 st	$g^2P^o-{}^2D$				
	Ar II	50.118 97 st	$g^2P^o-{}^2P$				
	Ar II	50.138 72 st	$g^2P^o-{}^2P$				
	Ar II	50.202 76 st	$g^2P^o-{}^2P$				
	Ar II	50.216 29 st	$g^2P^o-{}^4P$				
	Ar II	50.365 03 st	$g^2P^o-{}^2D$				
	Ar II	50.481 17 st	$g^2P^o-{}^2P$				
	Ar II	50.501 21 st	$g^2P^o-{}^2P$				
	Ar II	51.055 09 st	$g^2P^o-{}^2D$				
	Ar II	51.055 64 st	$g^2P^o-{}^2D$				
5	Ar II	51.431 00 st	$g^2P^o-{}^2D$	52.2	51.4–53.0	0.94	1.48[b]
	Ar II	51.890 88 st	$g^2P^o-{}^2D$				
	Ar II	51.932 69 st	$g^2P^o-{}^2D$				
	Ar II	52.279 24 st	$g^2P^o-{}^2D$				
	Ar II	52.468 03 st	$g^2P^o-{}^2P$				
	Ar II	52.649 69 st	$g^2P^o-{}^2P$				
	Ar II	52.865 11 st	$g^2P^o-{}^2P$				
	Ar II	53.049 54 st	$g^2P^o-{}^2P$				

Table 1 (continued).

No	Species	Wavelength (nm)	Term*	λ_{obs} (nm)	IWI (nm)	Cross section 200 eV	Other expts
6	Ar II	53.307 94 st	$g^2P^o-{}^2F$	54.3	53.4–55.2	2.24	−2.13[b]
	Ar II	53.507 11 st	$g^2P^o-{}^4P$				
	Ar II	53.713 96 st	$g^2P^o-{}^4P$				
	Ar II	53.741 93 st	$g^2P^o-{}^4F$				
	Ar II	54.080 66 st	$g^2P^o-{}^4F$				
	Ar II	54.130 19 st	$g^2P^o-{}^4P$				
	Ar II	54.291 23 st	$g^2P^o-{}^4D$				
	Ar II	54.320 32 st	$g^2P^o-{}^2S$				
	Ar II	54.350 8	$g^2P^o-{}^4D$				
	Ar II	54.373 05 st	$g^2P^o-{}^2P$				
	Ar II	54.617 68 st	$g^2P^o-{}^2P$				
	Ar II	54.716 50 st	$g^2P^o-{}^4D$				
	Ar II	54.746 05 st	$g^2P^o-{}^2S$				
	Ar II	54.799 60 st	$g^2P^o-{}^2P$				
	Ar II	54.878 08 st	$g^2P^o-{}^4P$				
	Ar II	55.048 10 st	$g^2P^o-{}^2P$				
	Ar II	55.090 45 st	$g^2P^o-{}^4P$				
7	Ar II	55.312 63	$g^2P^o-{}^4P$	55.8	55.2–56.4	0.65	
	Ar II	55.576 59	$g^2P^o-{}^2D$				
	Ar II	55.681 69	$g^2P^o-{}^2D$				
	Ar II	56.022 32	$g^2P^o-{}^2D$				
8	Ar II	57.201 36 st	$g^2P^o-{}^2P$	57.7	56.4–58.9	3.28	3.22[b]
	Ar II	57.336 19 st	$g^2P^o-{}^2P$				
	Ar II	57.673 64 st	$g^2P^o-{}^2P$				
	Ar II	57.810 71 st	$g^2P^o-{}^2P$				
	Ar II	57.860 43 st	$g^2P^o-{}^2D$				
	Ar II	58.026 31 st	$g^2P^o-{}^2D$				
	Ar II	58.343 71 st	$g^2P^o-{}^2D$				
9	Ar II	59.770 00 st	$g^2P^o-{}^2S$	59.8	58.9–60.9	0.85	
	Ar II	60.285 84 st	$g^2P^o-{}^2S$				
10	Ar II	61.237 15 st	$g^2P^o-{}^2F$	61.3	60.9–62.1	0.33	
11	Ar III	63.682	$g^3P-{}^3D^o$	64.0	62.9–65.2	0.28	
	Ar III	63.728	$g^3P-{}^3D^o$				
	Ar III	64.136	$g^3P-{}^3D^o$				
	Ar III	64.181	$g^3P-{}^3D^o$				
	Ar III	64.326	$g^3P-{}^3D^o$				
12	Ar II	66.186 87 st	$g^2P^o-{}^2D$	66.3	65.2–66.4	0.78	0.77[b]
	Ar II	66.456 22 st	$g^2P^o-{}^2D$				
	Ar II	66.601 08 st	$g^2P^o-{}^2F$				
13	Ar II	67.094 55 st	$g^2P^o-{}^2D$	67.2	66.4–67.6	2.43	
	Ar II	67.185 13 st	$g^2P^o-{}^2D$				
	Ar II	67.285 62 st	$g^2P^o-{}^2D$				
14	Ar II	67.624 24 st	$g^2P^o-{}^4P$	67.2	67.6–68.6	1.06	
	Ar II	67.795 18 st	$g^2P^o-{}^4P$				
	Ar II	67.921 83 st	$g^2P^o-{}^4P$				
	Ar II	67.940 05 st	$g^2P^o-{}^2D$				

Table 1 (continued).

No	Species	Wavelength (nm)	Term*	λ_{obs} (nm)	IWI (nm)	Cross section 200 eV	Other expts
15	Ar II	68.648 83 st	$g^2P^o-{}^2P$	69.4	68.6–70.8	0.85	
	Ar II	69.103 73 st	$g^2P^o-{}^2P$				
	Ar II	69.330 18 st	$g^2P^o-{}^2P$				
	Ar II	69.748 90 st	$g^2P^o-{}^4F$				
	Ar II	69.794 18 st	$g^2P^o-{}^2P$				
	Ar II	69.877 45 st	$g^2P^o-{}^4F$				
	Ar II	70.452 37 st	$g^2P^o-{}^4F$				
16	Ar II	71.808 98 st	$g^2P^o-{}^2P$	72.4	70.8–73.6	2.57	1.06[a]
	Ar II	72.336 05 st	$g^2P^o-{}^2P$				
	Ar II	72.554 85 st	$g^2P^o-{}^2P$				
	Ar II	73.092 97 st	$g^2P^o-{}^2P$				
17	Ar II	73.745 37 st	$g^2P^o-{}^4P$	74.4	73.6–75.0	0.82	
	Ar II	74.026 91 st	$g^2P^o-{}^4P$				
	Ar II	74.492 47 st	$g^2P^o-{}^4P$				
	Ar II	74.532 22 st	$g^2P^o-{}^4P$				
	Ar II	74.819 82 st	$g^2P^o-{}^4P$				
18	Ar III	76.915	$^1D-{}^1P^o$	77.1	75.0–78.1	0.66	
19	Ar I		$g^1S-ns3/2,nd3/2$ $g^1S-ns'1/2,nd'1/2$	79.8	78.1–80.3	2.69	
20	Ar I	80.459	Unclassified	80.8	80.3–81.2	2.05	
	Ar I	80.647	$g^1S-6d3/2[3/2]^0$				
	Ar I	80.687	$g^1S-8s3/2[3/2]^0$				
	Ar I	80.722	$g^1S-7s'1/2[1/2]^0$				
	Ar I	80.765	$g^1S-5d'1/2[3/2]^0$				
	Ar I	80.927	$g^1S-6d3/2[1/2]^0$				
21	Ar I	81.623	$g^1S-5d3/2[3/2]^0$	81.6	81.2–82.1	1.94	
	Ar I	81.647	$g^1S-7s3/2[3/2]^0$				
	Ar I	82.013	$g^1S-5d3/2[1/2]^0$				
	Ar	82.098	Unclassified				
22	Ar I	82.535	$g^1S-6s'1/2[1/2]^0$	82.6	82.12–83.0	1.89	
	Ar I	82.636	$g^1S-4d'1/2[3/2]^0$				
23	Ar I	83.4392	$g^1S-4d3/2[3/2]^0$	83.5	83.0–84.2	1.91	
	Ar I	83.500	$g^1S-6s3/2[3/2]^0$				
	Ar I	84.281	$g^1S-4d3/2[1/2]^0$				
24	Ar I	86.680	$g^1S-3d'1/2[3/2]^0+$	86.7	85.5–87.2	6.24	1.26[a]
	Ar I	86.975	$g^1S-5s'1/2[1/2]^0$				
25	Ar I	87.606	$g^1S-3d3/2[3/2]^0+$	87.7	87.2–89.4	7.52	1.32[a]
	Ar I	87.995	$g^1S-5s3/2[3/2]^0$				
	Ar I	89.350	Unclassified				
	Ar I	89.431	$g^1S-3d3/2[1/2]^0$				
26	Ar II	91.978 st	$g^2P^o-{}^2S$	92.0	91.1–92.06	5.30	2.19[a] 3.82[b] 3.8[f] 5.5[g] 2.77[h]

Table 1 (continued).

No	Species	Wavelength (nm)	Term*	λ_{obs} (nm)	IWI (nm)	Cross section 200 eV	Other expts
27	Ar II	93.205 st	$g^2P^o-{}^2S$	93.2	92.6–93.9	2.68	1.24[a] 1.66[b] 1.96[f] 2.75[g] 1.41[h]
28	Ar I	104.822	g^1S–4s′1/2[1/2]^0	104.8	103.5–105.7	23.1Δ	14.9[a] 16.0[c] 16.5[d] 17.9[e] 12.81[f]
29	Ar I	106.666	g^1S–4s3/2[3/2]^0	106.7	105.7–107.3	9.32	6.11[a] 6.3[c] 6.5[d] 5.32[f]

[a] Mentall and Morgan (1976), corrected as indicated in text by factor of 0.62.
[b] Tan *et al* (1974), Tan and McConkey (1974a).
[c] McConkey and Donaldson (1973).
[d] Jongh (1971).
[e] Ganas and Green (1971).
[f] Forand *et al* (1988).
[g] McPherson (1984), see Forand *et al* (1988).
[h] Li *et al* (1988b).

cross sections of the $(^2P^o_{1/2})4s'$ state and the $(^2P^o_{3/2})4s$ state. They indicate the latter state, the upper state for the 106.7 nm transition, may have a cascading cross section of order 5%. We will show in the discussion section that the cascading cross section is indeed much larger. Strong evidence of this fact is the strength of the Rydberg series for ns, ns' ($n > 4$) in table 1 and figure 3 for feature numbers 19–25. The various Rydberg series and transitions are shown in the energy level diagram in figure 4 adapted from the Grotrian diagrams of Bashkin and Stoner (1978). The ground state of Ar is $3s^23p^6\ {}^1S_0$. The Ar I excited states have $3p^5$ cores with one electron excited to the 4s (106.7 nm) or 4s′ (104.8 nm) level, when the angular momentum of the core is $J_c = 1/2$ or 3/2, respectively.

4. Excitation functions for the Ar I, II resonance lines

We show in figures 5 and 6 the excitation function of Ar II(91.98 nm) over the energy ranges 0 to 400 eV and 0 to 2 keV respectively. Table 2 lists the emission cross section of Ar II(91.98 nm) and Ar(93.21 nm) from threshold 0 to 2 keV.

A comparison with other published results of Ar II(91.98 nm) emission cross sections is given in figure 7 which demonstrates that the comparison with M84 is excellent at 200 eV and shows that the relative shapes measured in this work and Tan *et al* (1974) are in satisfactory agreement. A complete discussion of the unusual shape of the emission cross section of this transition along with other Ar II transitions is given in a series of papers by the experimenters at the University of Windsor (Tan *et*

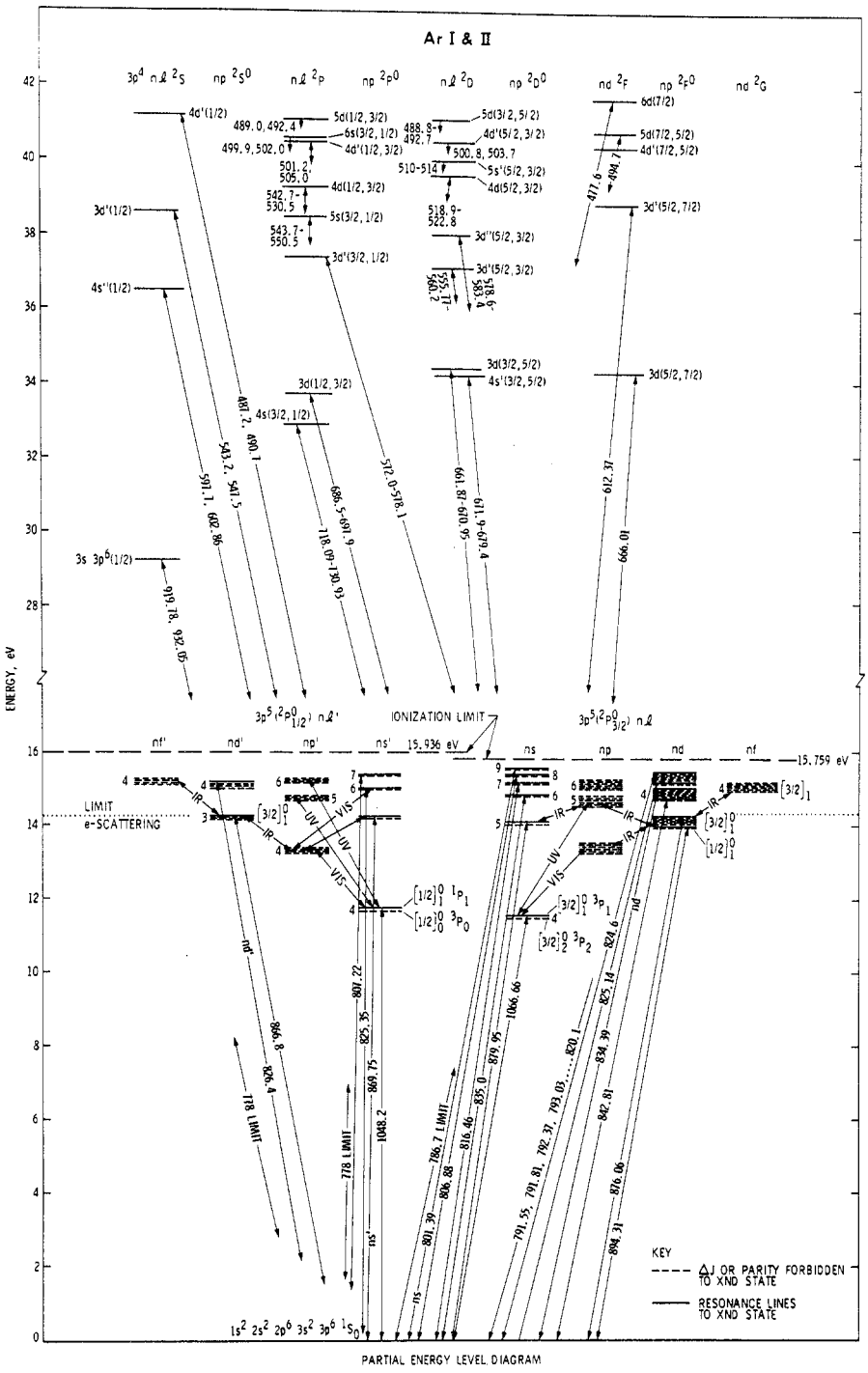

Figure 4. Partial energy level diagram for Ar I, II from Bashkin and Stoner (1978). Important transitions are given in ångströms. The high-energy-limit electron energy loss results of Chutjian and Cartwright (1981) is shown.

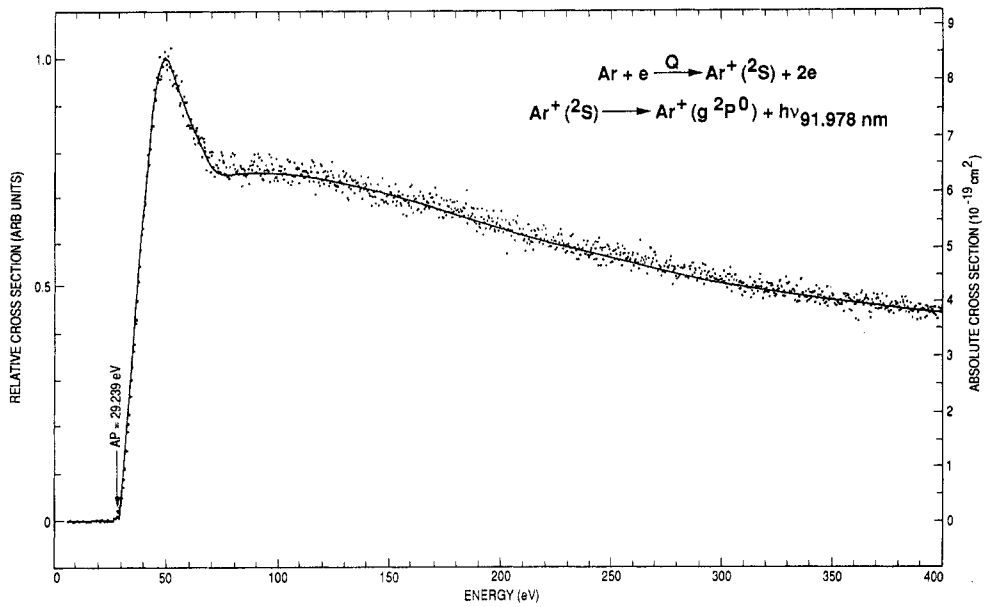

Figure 5. Relative and absolute emission cross sections of the Ar II(91.98 nm) transition from electron impact ionization–excitation of Ar over an energy range from 0 to 400 eV. Data points are taken every ~ 0.4 eV. The resolution of the spectrometer was 0.3 nm.

al 1974, Tan and McConkey 1974a, b). Configuration interaction is known to affect the $3s3p^6\ ^2S_{1/2}$ state. The wavefunction of the state is an admixture of $3s^23p^43d'$ and $3s^23p^44d'$ states, among others. These last two states are optically forbidden from the Ar ground state ($3s^23p^6$). To excite these levels requires a two-electron transition—one 3p electron escapes to the continuum and the other 3p electron is excited to a higher level. In fact most of the Ar II transitions in table 1 are of the two-electron excitation form and have excitation functions in the high-energy region that demonstrate optically forbidden behaviour (Tan and McConkey 1974a, b). Three exceptions found by Tan and McConkey are the $3s3p^6$ (91.98, 93.21 nm), $3s^23p^43d'$ and $3s^23p^44d'$ levels, at least over their energy range of 0 to 2 keV. In addition the excitation function for Ar II(91.98 nm) displays a double maximum separated by a shallow minimum. The sharp autoionization peak occurs at 48 eV in our experiment. The principle ionization peak occurs at 100 eV. Later studies by Tan *et al* (1974) show the Born region for Ar II(91.98 nm) is not attained until ~ 2.0 keV. Luyken *et al* (1972) find similar behaviour in their 0 to 20 keV study of the combined 91.98 nm and 93.21 nm emission cross section. They attribute the high energy for applicability of the Born approximation to the high binding energy of the inner-shell 3s electron involved in the ionization–excitation process. Beginning at about 2 keV the slope of the collision strength ($Q\epsilon$) versus ln ϵ, where ϵ is the energy and Q is the cross section, becomes constant, indicating the dominance of an optically forbidden process from configuration interaction at asymptotically high energies (Tan *et al* 1974, Tan and McConkey 1974a, b).

The renormalized cross sections of McConkey and Donaldson (1973) for Ar I(104.8 nm) and Ar I(106.7 nm) are shown in figure 8. A simple increase of the

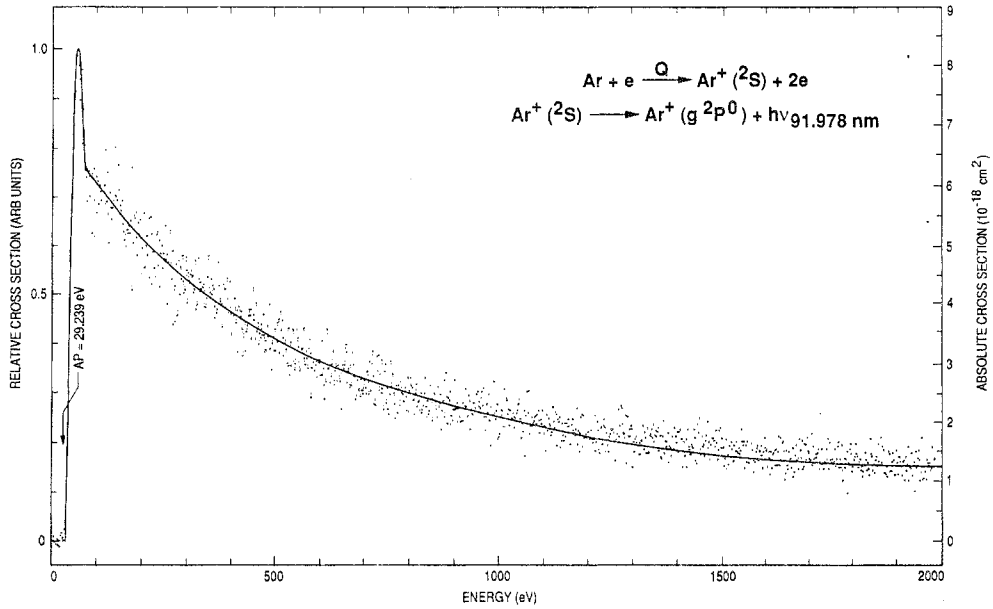

Figure 6. Relative and absolute emission cross sections of the Ar II(91.98 nm) transition from electron impact ionization–excitation of Ar over an energy range from 0 to 2 keV. Data points are taken every ~ 0.4 eV. The resolution of the spectrometer was 0.5 nm.

Table 2. Emission cross sections of Ar II (91.98 nm, 93.21 nm) transitions.

Energy	Cross section (10^{-18} cm^2)		Energy	Cross section (10^{-18} cm^2)	
(eV)	91.98 nm	93.21 nm	(eV)	91.98 nm	93.21 nm
29.2	0	0	500	3.23	1.63
30	0.41	0.21	600	2.98	1.51
40	5.71	2.89	700	2.65	1.34
50	8.28	4.19	800	2.32	1.17
60	7.37	3.73	900	2.15	1.09
70	6.37	3.22	1000	1.99	1.01
80	6.25	3.16	1100	1.86	0.94
90	6.29	3.19	1200	1.70	0.86
100	6.25	3.16	1300	1.57	0.79
120	6.13	3.10	1400	1.47	0.74
150	5.88	2.97	1500	1.42	0.72
200	5.30	2.68	1600	1.35	0.68
250	4.80	2.43	1700	1.30	0.66
300	4.31	2.18	1800	1.24	0.63
350	4.02	2.03	1900	1.22	0.62
400	3.81	1.93	2000	1.20	0.61

McConkey and Donaldon values by 44% and 47% for the 104.8 nm and 106.7 nm transitions, respectively, translates into the corrected results. Table 3 lists the emission cross sections of 104.8 nm and 106.7 nm transitions from threshold 0 to 2 keV, reflecting this correction. Figure 8 also shows the comparison with other published emission

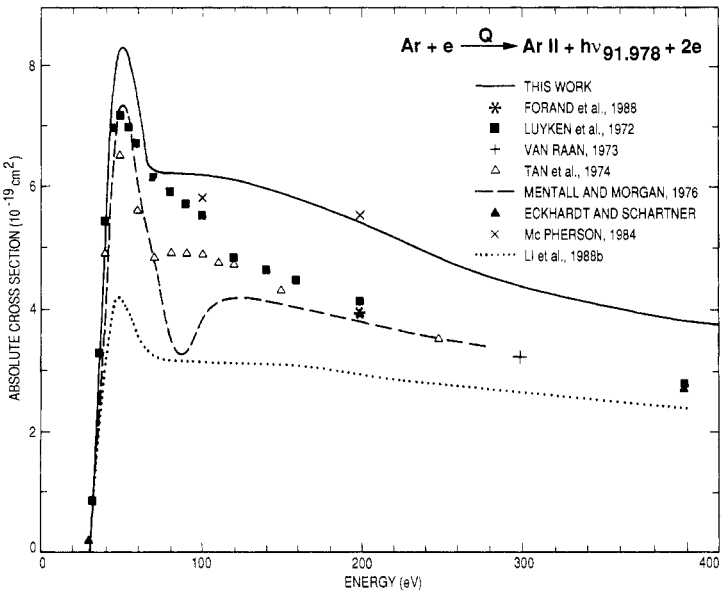

Figure 7. Comparison of published data for the emission cross section of the Ar II(91.98 nm) transition from electron impact ionization–excitation of Ar from 0–400 eV. Measurements shown are: ——, this work; ■, Luyken *et al* (1972); +, van Raan (1973); △, Tan *et al* (1974); – – –, Mentall and Morgan (1976); ▲, Eckhardt and Schartner (1983); ×, McPherson (1984); ∗, Forand *et al* (1988) and · · · · · ·, Li *et al* (1988b).

Table 3. Emission cross sections of Ar I (104.8 nm, 106.7 nm) transitions.

Energy	Cross section (10^{-18} cm^2)		Energy	Cross section (10^{-18} cm^2)	
(eV)	104.8 nm	106.7 nm	(eV)	104.8 nm	106.7 nm
12	0.85	2.43	100	31.2	13.5
14	8.81	12.0	120	29.4	12.2
16	15.6	16.0	150	26.6	10.8
20	27.1	24.3	200	23.1	9.32
24	34.1	30.6	250	20.3	8.20
28	37.5	32.8	300	18.2	7.38
30	38.0	32.4	400	15.0	6.09
35	37.9	27.5	500	12.0	5.22
40	37.3	22.6	600	11.3	4.57
45	36.8	18.8	800	8.93	3.61
50	36.1	17.8	1000	7.44	3.00
60	35.0	16.6	2000	4.27	1.72
80	33.0	14.8			

and direct excitation cross sections. McConkey and Donaldson find the 104.8 nm transition has a peak cross section at ~ 30 eV and the 106.7 nm transition has a peak cross section at ~ 28 eV. Cascading must be very important at all energies. Figure 8 shows the comparison of the direct excitation cross sections of Li *et al* (1988b) and Chutjian and Cartwright (1981) with the emission cross section of this work based on the renormalization described above. There are no direct excitation cross section

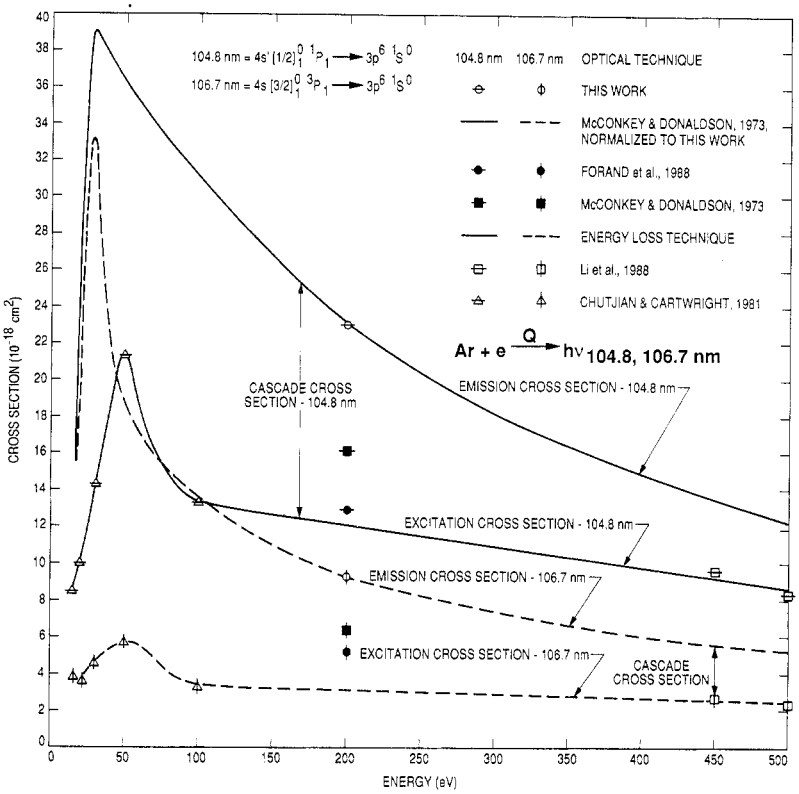

Figure 8. Comparison of emission and excitation cross sections of the Ar I resonance lines at 104.8 nm and 106.7 nm from 0–500 eV.

measurements in the energy range 100 to 400 eV. We schematically indicate the direct excitation cross section by drawing a straight line between the last data point of Chutjian and Cartwright and the high-energy (400, 500 eV) data points of Li *et al.* The difference between the two curves indicates that the percentages of cascading and direct excitation are roughly equal at all energies for both resonance transitions. In the low-energy range (0 to 50 eV) cascading to the 106.7 nm dramatically increases to almost 75% of the measured emission cross section. A more precise study of the cascading contribution at 100 eV to the 106.7 nm transition will be made in the discussion section. The types of transitions include: (i) permitted two-step (ns,nd–np–4s) cascading transitions and, (ii) parity forbidden excitation process followed by one step ($3p^6$–np–4s) cascading transitions to the 4s state shown in figure 4. A similar sequence exists for the 4s′ level. In addition, intercombination lines exist between the two $J_c = 1/2, 3/2$ JJ-coupled systems (Wiese *et al* 1969). Our measurement of the 106.7 nm cross section allows a renormalization of the Li *et al* (1988a) results. These authors use the direct excitation cross section of 106.7 nm at 500 eV of 2.23×10^{-18} cm^2 as an estimate of the emission cross section to normalize their emission cross section measurement of Ar II(91.98 nm). Our estimate of the Ar I(106.7 nm) cross section at 500 eV is 5.22×10^{-18} cm^2. Thus the Ar II(91.98 nm) cross section of Li *et al* must be increased by a factor of 2.34. The renormalized value of Li *et al* (1988a)

for the Ar II(91.98 nm) emission cross section is 4.82×10^{-18} cm^2 at 500 eV. This normalization value determines the 200 eV cross section of $6.8 \pm 1.3 \times 10^{-18}$ cm^2 from the excitation function presented here. The original error bars of Li *et al* (1988a) are used to give the uncertainty. The Li *et al* revised value is approximately 28% larger than our value at 200 eV. The two experiments now agree within the overlap of the combined error bars.

5. The FUV spectrum

We show in figure 9 the FUV spectrum of Ar at 1.0 nm resolution over the wavelength range 110–210 nm. The FUV spectrum consists entirely of Ar II features. A complete identification of these features is given in Kelly (1987). Some identifications are given in figure 9. We list in table 4 the relative cross sections of these features. A relative-flow study of features 5–8 places an upper limit on the combined cross section of 1×10^{-19} cm^2 at 200 eV.

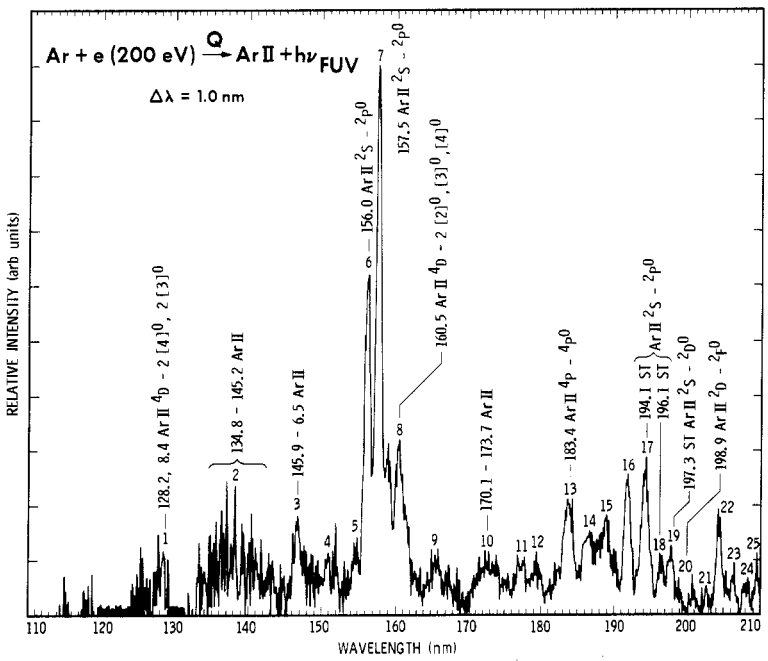

Figure 9. Calibrated, optically thin electron impact induced fluorescence spectrum at 200 eV impact energy at a resolution of 1.0 nm. The spectrum was obtained in the crossed-beam mode at 1×10^{-5} Torr background pressure. All of the numbered features are identified in table 4 from Kelly (1987).

6. Discussion

The most fundamental result of this paper is the absolute emission cross section of the Ar II resonance lines using the relative-flow technique developed at the Jet Propulsion

Table 4. Relative argon emission cross sections in the FUV at 200 eV electron impact energy and $\Delta\lambda = 1.0$ nm.

Feature no	Species†	Observed peak wavelength (nm)	Integrated wavelength interval (nm)	Relative cross section
1	Ar II	127.6	126.8–129.3	0.309
2	Ar II	136.9	132.6–144.0	2.107
3	Ar II	146.6	144.0–149.0	0.910
4	Ar II	150.8	149.0–152.9	0.646
5	Ar II	154.7	152.9–155.2	0.452
6	Ar II	156.2	155.2–156.7	1.596
7	Ar II	158.9	156.7–159.6	3.618
8	Ar II	160.5	159.6–163.8	1.655
9	Ar II	165.8	163.8–169.6	0.729
10	Ar II	172.7	169.6–174.3	0.742
11	Ar II	176.6	174.3–177.9	0.558
12	Ar II	179.2	177.9–180.5	0.402
13	Ar II	183.5	180.5–185.0	1.184
14	Ar II	186.5	185.0–187.3	0.701
15	Ar II	188.8	187.3–190.7	1.010
16	Ar II	191.7	190.7–192.5	0.759
17	Ar II	194.2	192.5–195.5	0.994
18	Ar II	196.1	195.5–197.0	0.271
19	Ar II	197.7	197.0–198.7	0.352
20	Ar II	200.6	198.7–201.8	0.053
21	Ar II	202.5	201.8–203.2	0.052
22	Ar II	204.1	203.2–205.4	0.483
23	Ar II	206.3	205.9–207.0	0.110
24	Ar II	207.9	207.0–208.8	0.102
25	Ar II	209.4	208.8–210.0	0.132
Sum of 1–25	Ar II		126.8–210.0	19.93

† Complete identification given in Kelly (1987).

Laboratory (Srivastava *et al* 1975, Trajmar and Register 1984). In this method the N I(120.0 nm) fluorescence signal from N_2, the standard gas is compared with the fluorescence signal from Ar II(91.98 nm) the unknown gas, at 200 eV. These comparisons are made over a range of background gas pressures from 1×10^{-7} Torr to 1×10^{-5} Torr to establish linearity of the signal with pressure. The cross section of the N I(120.0 nm) multiplet was previously measured to be $3.11 \pm 0.31 \times 10^{-18}$ cm^2 (Ajello *et al* 1989, Ajello and Shemansky 1985). On this basis we find the emission cross section of the Ar II(91.98 nm) line to be $5.3 \pm 0.7 \times 10^{-18}$ cm^2.

This value agrees to within 4% of the value of $5.5 \pm 0.4 \times 10^{-18}$ cm^2 measured by M84. Similarly the cross section of the Ar II line at 93.21 nm was measured to be $2.68 \pm 0.04 \times 10^{-18}$ cm^2. The ratio of these two lines is 1.98 : 1 which, within the experimental error, is the ratio of the statistical weights of the lower state. The two lines originate from the same upper level and the measured shape of the excitation functions are found to be identical (Tan *et al* 1974).

The relative-flow results on the Ar II resonance line at 91.98 nm represent confirmation of a major change of about 50% in the set of previously accepted values of this cross section. The first major application of this new cross section value of

$5.3 \pm 0.7 \times 10^{-18}$ cm^2 at 200 eV is the determination of the cross section of the Ar I resonance lines at 104.8 nm and 106.7 nm. The values for these features were about 50% higher than previous estimates (McConkey and Donaldson 1973, F88). The major inference of the emission cross section values is that large cascading cross sections are needed to reconcile the direct excitation cross section values of Chutjian and Cartwright (1981) and Li *et al* (1988a, b) with the results presented here.

Table 5. Evidence for strong cascading contributions to $4s[3/2]_1^0$ $^3P_1$ 106.7 nm resonance line. (*a*) Electron energy loss Ar I states below 14.3 eV. (*b*) This work optical emission technique: Ar I states between 14.3 and 15.8 eV. Cross sections are given in 10^{-19} cm^2.

(*a*) Upper level[b]	Line no[b] (partitioning)	Q_{ex}(X)[c]	Q_{em}(X)[d]	Q_{cas}[d]	Laporte rule[e] ground state	λ_{dir}[f] (nm)
			100 eV			
*n*s Rydberg series, $n > 4$						
$5s[3/2]_1^0$	19 (2)	7.4	4.6	2.8	a	87.995
$5s[3/2]_2^0$	18 (2)	1.2	0	1.2	f	
*n*p Rydberg series						
$4p[1/2]_0$	10 (2)	2.28	0	2.28	f	
$4p[1/2]_1$	5	0.54	0	0.54	f	
$4p[5/2]_3$	6	0.93	0	0.93	f	
$4p[5/2]_2$	7	6.73	0	6.73	f	
$4p[3/2]_1$	8	1.93	0	1.93	f	
$4p[3/2]_2$	9	5.89	0	5.89	f	
*n*d Rydberg series						
$3d[3/2]_1^0$	20	34.3	26.8	7.5	a	87.606
$3d[5/2]_3^0$	19 (2)	7.4	0	7.4	f	
$3d[5/2]_{2,3}^0$	18 (2)	1.2	0	1.2	f	
$3d[7/2]_3^0$	17	2.01	0	2.01	f	
$3d[7/2]_4^0$	16	0.90	0	0.90	f	
$3d[3/2]_2^0$	15	1.42	0	1.42	f	
$3d[1/2]_{0,1}^0$	14	1.51	1.18	0.33	a	89.431

(*b*) Upper level[g]	Lower level[g]	Line no[g]	Q_{em}[g] 200 eV	Q_{em}[h] 100 eV	Q_{cas}[i] 100 eV	λ_{dir}[f] (nm)
*n*s3/2, *n*d3/2	g^1S	19 (2)	13.5	19.7	8.4	
8s 3/2[3.2]^0	g^1S	20 (2)	10.3	15.0	6.4	80.687
6d 3/2[1/2]^0						80.927
7s 3/2[3/2]^0	g^1S	21	19.4	28.03	12.0	81.647
5d 3/2[3/2]^0						81.623
5d 3/2[1/2]^0						82.013
6s 3/2[3/2]^0	g^1S	23	19.1	27.9	12.0	83.500
4d 3/2[3/2]^0						83.4392
4d 3/2[1/2]^0						82.281
Overlap with energy loss						
5s 3/2[3/2]^0	g^1S	25	75.2	110.0	47.1	87.995
3d 3/2[3/2]^0						87.606
3d 3/2[1/2]^0						89.431

Table 5 (continued).

100 eV: summary for 106.7 nm

Total cascade np(electron scattering) + (ns + nd) (optical emission) = 104 x 10^{-19} cm^2.
Compared with:

Q_{em} (106.7 nm) = 135 x 10^{-19} cm^2 (this work)
Q_{dir} (106.7 nm) = 32.8 x 10^{-19} cm^2 (Chutjian and Cartwright 1981)
Q_{casc} (106.7 nm) = 102 x 10^{-19} cm^2 from the relation $Q_{em} = Q_{dir} + Q_{casc}$.

100 eV: summary for 104.8 nm (detailed table not shown for 4s'[1/2]^0, ^{1}P$_1$)

Total cascade np' (electron scattering) + (ns' + nd') optical emission = 25.9 + 72 ≅ 98 x 10^{-19} cm^2

Q_{em} (104.8 nm) = 312 x 10^{-19} cm^2 (this work)
Q_{dir} (104.8 nm) = 134 x 10^{-19} cm^2 (Chutjian and Cartwright 1981)
Q_{casc} (104.8 nm) = 178 x 10^{-19} cm^2 from the relation $Q_{em} = Q_{dir} + Q_{casc}$.

[a] Chutjian and Cartwright (1981).

[b] Upper level and line number from Chutjian and Cartwright (1981). The partitioning factor, in brackets, is arbitrarily set at 2 when ns and nd Rydberg features are blended. The measured cross section is divided by 2 with half the cross section value for the ns and half for the nd feature.

[c] The measured direct excitation cross section of Chutjian and Cartwright.

[d] The excitation cross section branches in emission into an emission cross section to ground state ^{1}S$_0$ and into an emission cross section via the allowed 5s–4p or 3d–4p transitions. This branching defines a cascade cross section contribution to the 4p level. The average branching ratio from Wiese *et al* (1969) is 0.38 for 5s → 4p and 0.22 for 3d → 4p for 5s and 3d terms respectively.

[e] Laporte rule for JJ coupling $\Delta l = \pm 1$, $\Delta J = 0, \pm 1$, $J = 0 \not\rightarrow J = 0$ with a = allowed, f = forbidden.

[f] Direct excitation emission wavelength to ground state from Kelly (1987).

[g] Upper and lower levels, emission cross sections and line numbers are given in table 1.

[h] emission cross section at 100 eV estimated from 106.7 nm excitation function which gives Q_{em}(100 eV)/Q_{em}(200 eV) = 1.45 and from 104.8 excitation function which gives Q_{em}(100 eV)/Q_{em}(200 eV) = 1.35.

[i] Cascade cross section at 100 eV is estimated from average cascade branching ratio ω_{casc} ≅ 0.30, for ns and nd based on Wiese *et al* (1969).

As evidence for the large cascading contribution to the Ar I resonance lines we now provide a detailed study of the cascading cross section contributions to the 4s[3/2]$^0_1$ ^{3}P$_1$–^{1}S$_0$ 106.7 nm resonance line. We consider the cascade cross sections at 100 eV, the highest energy studied by Chutjian and Cartwright (1981) in their electron energy loss technique. These authors studied the states below 14.3 eV. We list in table 5(a) the cascade cross sections to the 4s state for the 106.7 nm line. The cascade cross sections are based on the direct excitation cross sections of Chutjian and Cartwright for the Rydberg series members with n = 5. The Rydberg series contributing to cascade transitions include the ns, np and nd series with $n > 4$ (3 for the nd series). The branching ratio for n = 5s, 3d states are calculated from transition probabilities given in Wiese *et al* (1969). To account for the Rydberg series members in the ns and nd series, we make use of the emission cross sections measured in this work for feature numbers 19–25. We provide estimates of the cascade cross sections for ns, nd with $n >$ 5s or 3d in table 5(b). The numbers are approximate because we make the following assumptions: (i) the 100 eV cross section for the higher Rydberg series members are in the same ratio to the 200 eV cross section as the 106.7 nm cross section in table 3; and (ii) the branching ratio for the higher members to 4s is the same as for the 5s, 3d members to 4s in table 5(a). The only states not accounted for in this scheme are the optically forbidden np series with $n > 4$ (states above 14.3 eV). Direct excitation of np series from the ground state requires $\Delta l = 0$ transitions. These

transitions are not strictly forbidden due to configuration interaction (da Paixao *et al* 1984). The results described at the bottom of table 5 summarize the important cross sections. We find the emission cross section of 106.7 nm to be 135×10^{-19} cm^2, compared with the direct excitation cross section of 32.8×10^{-19} cm^2 measured by Chutjian and Cartwright (1981). The cascade cross section is the difference of these two results and this yields a value of 102×10^{-19} cm^2. At the same time all the different components to the cascade cross section delineated in table $5(a, b)$ yield a value of 104×10^{-19} cm^2. The agreement is quite remarkable and implies the result that cascade contributions to the 106.7 nm resonance line dominate direct cross sections at 100 eV. The result stems from the weak decline of cross section with principal quantum number in distinction to the hydrogenic $1/n^3$ decrease.

A similar summary is given for 104.8 nm at the bottom of table 5. The difference between the two estimates of cascading is more substantial: 178×10^{-19} cm^2 (difference emission–direct) versus 98×10^{-19} cm^2 (itemized electron energy loss + optical emission). However the itemized results from table 5 do not include members of the np series higher than $n = 4$ and intercombination transitions listed in Wiese *et al* (1969) are omitted. A more meaningful comparison may be made by considering the results for the combined 4s+ 4s′ states. A comparison of the sums of the itemized results for the cascade to the 4s + 4s′ states generates a value of cascading of 202×10^{-19} cm^2 compared with the required 280×10^{-19} cm^2. This difference can be accommodated by the omitted np, np' $n > 4$ Rydberg series emission cross sections.

Acknowledgments

This work is supported by the US Air Force Office of Scientific Research (AFOSR), the Aeronomy Program of the National Science Foundation Grant No ATM8715709 and NASA Planetary Atmospheres and Astronomy /Astrophysics Program Offices, under Contract No NAS7-100 to the Jet Propulsion Laboratory, California Institute of Technology. We greatly appreciate the digital cross section data and careful review of the manuscript provided by W McConkey and S Trajmar. Computer graphics were kindly provided by K Ivanoff.

References

Ajello J M, James G K, Franklin B O and Shemansky D E 1989 *Phys. Rev.* A **40** 3524
Ajello J M and Shemansky D E 1985 *J. Geophys. Res.* **90** 9845
Ajello J M, Shemansky D, Kwok T L and Yung Y L 1984 *Phys. Rev.* A **29** 636
Ajello J M, Srivastava S K and Yung Y L 1982 *Phys. Rev.* A **25** 2485
Ajello J M *et al* 1988 *Appl. Opt.* **27** 890
Bashkin S and Stoner J O Jr 1978 *Atomic Energy-Levels and Grotrian Diagrams* vol 2 *Sulfur I-Titanium XXII* (Amsterdam: North-Holland) p 166
Broadfoot A L *et al* 1979 *Science* **204** 979
—— 1986 *Science* **233** 74
Chutjian A and Cartwright D C 1981 *Phys. Rev.* A **23** 2178
da Paixao F J, Padial N T and Csanak G 1984 *Phys. Rev.* A **30** 1697
Dassen H, Malcolm I C and McConkey J W 1977 *J. Phys. B: At. Mol. Phys.* **10** L493
Eckhardt M and Schartner H-H 1983 *Z. Phys.* A **312** 321
Forand J L, Wang D, Woolsey J M and McConkey J W 1988 *Can. J. Phys.* **60** 349
Ganas P S and Green A E S 1971 *Phys. Rev.* A **4** 182
Jongh J P 1971 *PhD Thesis* University of Utrecht Netherlands unpublished

Kelly R L 1987 *J. Phys. Chem. Ref. Data* **16** 1
Khakoo M A and McConkey J W 1986 *Phys. Rev. Lett.* **57** 679
Lawrence G M 1969 *Phys. Rev.* **179** 134
Li G P, Takayanagi T, Wakiya K and Suzuki H 1988a *Phys. Rev.* A **38** 1831
Li G P, Takayanagi T, Wakiya K, Suzuki H, Ajiro T, Yagi S, Kano S S and Takuma H 1988b *Phys. Rev.* A **38** 1240
Lloyd C R, Teubner P J O, Weigold E and Hood T S 1972 *J. Phys. B: At. Mol. Phys.* **5** L44
Luyken B F J, de Heer F J and Baas R Ch 1972 *Physica* **61** 200
McConkey J W and Donaldson F G 1973 *Can. J. Phys.* **51** 914
McPherson A 1984 *PhD Thesis* North Carolina State University, Raleigh, NC unpublished
Mentall J E and Morgan H D 1976 *Phys. Rev.* A **14** 954
Risley J S and Westerveld W B 1989 *Appl. Opt.* **28** 389
Sandel B R *et al* 1982 *Science* **215** 553
Sawada T, Purcell J E and Green A E S 1971 *Phys. Rev.* A **4** 193
Shemansky D E, Ajello J M and Hall D T 1985a *Astrophys. J.* **296** 765
Shemansky D E, Ajello J M, Hall D T and Franklin B 1985b *Astrophys. J.* **296** 774
Srivastava S K, Chutjian A and Trajmar S 1975 *J. Chem. Phys.* **7** L183
Tan K-H and McConkey J W 1974a *J. Phys. B: At. Mol. Phys.* **7** L183
—— 1974b *Phys. Rev.* A **10** 1212
Tan K-H, Donaldson F G and McConkey J W 1974 *Can. J. Phys.* **52** 786
Trajmar S and Register D 1984 *Electron Molecular Collisions* ed K Takayanagi and I Shimamura (New York: Plenum) ch 6
van der Burgt P J M, Westerveld W B and Risley J S 1989 *J. Chem. Phys. Ref. Data* **18** 1757
van Raan A F J 1973 *Physica* **65** 566
Wiese W L, Smith M W and Miles B M 1969 *Atomic Transition Probabilities* vol 2 *Sodium Through Calcium* (NSRDS-NBS 22) (Washington, DC: US Govt Printing Office) p 187